

## Thermal history of solid $^4\text{He}$ under oscillation

A. C. Clark,\* J. D. Maynard, and M. H. W. Chan

*Department of Physics, The Pennsylvania State University, University Park, Pennsylvania 16802, USA*

(Received 13 January 2008; revised manuscript received 21 April 2008; published 19 May 2008)

We have studied the thermal history of the resonant frequency of a torsional oscillator containing solid  $^4\text{He}$ . We find that the magnitude of the frequency shift that occurs below  $\sim 100$  mK is multivalued in the low-temperature limit, depending strongly on how the state is prepared. This result can be qualitatively explained in terms of the motion and pinning of quantized vortices within the sample. Several aspects of the data are also consistent with the response of dislocation lines to oscillating stress fields imposed on the solid. However, studies of solid helium in porous media, several control experiments, and the magnitude of the frequency shift found in this and other experiments all indicate that the most appropriate interpretation of the torsional oscillator results is the existence of a supersolid  $^4\text{He}$  phase.

DOI: [10.1103/PhysRevB.77.184513](https://doi.org/10.1103/PhysRevB.77.184513)

PACS number(s): 67.80.-s, 61.72.Lk, 74.25.Qt

### I. INTRODUCTION

Over the last several years the torsional oscillator (TO) technique has become a popular method<sup>1–12</sup> to study solid  $^4\text{He}$ . The measurements, which involve monitoring the resonant frequency  $f$  of a high-quality factor torsion pendulum filled with  $^4\text{He}$ , have revealed a “transition” below an onset temperature  $T_o$  of a few hundred millikelvin. The results of several control experiments<sup>2</sup> indicate that the sudden increase in the frequency is due to a superfluidlike decoupling of a fraction of the  $^4\text{He}$  mass. The apparent nonclassical rotational inertia fraction (NCRIF), proportional to the frequency shift  $\delta f$ , is independent<sup>2</sup> of the maximum oscillation speed  $v_0$  of the TO provided that it is smaller than a critical value. Above this critical velocity  $v_c$  the magnitude of the NCRIF is attenuated. The value of  $v_c$  corresponds to several quanta of circulation  $\kappa$ , suggesting that the important excitations in the system are vortices. Anderson has proposed<sup>13</sup> a vortex liquid model that qualitatively captures a number of experimental results.

In multiple solid  $^4\text{He}$  samples slowly grown within an annulus of radius  $r=5$  mm and width,<sup>14</sup>  $t=0.95$  mm, a value of  $v_c=10$   $\mu\text{m s}^{-1}$  was found<sup>4</sup> (corresponding to  $\kappa=2\pi r v_0 \approx 3h/m$ , where  $h$  is Planck’s constant and  $m$  is the bare  $^4\text{He}$  mass). The NCRIF decreased almost linearly with  $\ln[v_0]$  as the speed was increased further. This attenuation, according to Ref. 13, could be attributed to the nonlinear susceptibility of a vortex liquid phase, which consists of an entanglement of many thermally activated vortices. The ability of the vortices to move counter to the time-dependent superflow (relative to the cell’s oscillation) results in the screening of supercurrents. As the temperature is lowered, the motion and number of vortices are reduced so that the NCRIF becomes finite. The accompanying dissipation<sup>2</sup> that peaks in the middle of the transition is due to a matching of  $f$  and the optimal rate at which vortices respond to changes in the velocity field. Residual  $^3\text{He}$  atoms may<sup>15</sup> cling to vortices, thereby slowing vortex motion and ultimately enhancing the onset temperature.<sup>1,10,11</sup>

One prediction of Anderson’s model<sup>13</sup> is that  $T_o$ , and perhaps NCRIF, for a particular sample will decrease as the measurement frequency is lowered. Aoki *et al.* performed<sup>7</sup>

measurements in a double oscillator that operated in either an antisymmetric (high- $f$ ) or a symmetric (low- $f$ ) mode and found that for the same  $^4\text{He}$  sample,  $T_o \approx 240$  mK at 1173 Hz and  $T_o \approx 160$  mK at 496 Hz. However, the NCRIF became independent of frequency below  $\sim 35$  mK. In addition, irreversible changes in NCRIF below  $\sim 45$  mK occurred upon variation of the oscillation speed between  $10$   $\mu\text{m s}^{-1}$  and  $800$   $\mu\text{m s}^{-1}$ .

Nonsuperfluid explanations of the TO experiments have also been proposed, in which some sort of freezing process<sup>16</sup> or glass transition<sup>17</sup> takes place. The pinning of dislocation lines within solid  $^4\text{He}$  is one possible realization of such a “freezing” transition. The mechanism for dislocation pinning is likely related to interactions with isotopic impurities. It is known that dislocations<sup>18</sup> and  $^3\text{He}$  atoms<sup>19,20</sup> are mobile in solid  $^4\text{He}$  below  $\sim 1$  K, but the strong coupling between them in the low-temperature limit can immobilize them both.<sup>21,22</sup> In a TO study<sup>11</sup> of many solid  $^4\text{He}$  samples we found that the dependence of  $T_o$  on the  $^3\text{He}$  concentration  $x_3$  is quantitatively consistent with this impurity pinning model.

Recently Day and Beamish observed<sup>23</sup> a dramatic increase (between 5% and 20%) in the shear modulus  $c_{44}$  of solid  $^4\text{He}$  ( $x_3 \approx 0.3$  ppm) below  $\sim 250$  mK, with the temperature dependence of  $c_{44}$  strongly resembling that of  $f$  in TO experiments. The authors also reported hysteresis in  $c_{44}$  upon adjusting the stress amplitude of the measurement at  $T \approx 20$  mK, similar to what is seen in Ref. 7. The increase in the shear modulus is very likely due to the stiffening of the dislocation network via the immobilization of individual lines. It was suggested by the authors of Ref. 23 that an increase in  $c_{44}$  will result in a stronger coupling between the  $^4\text{He}$  sample and its container and therefore mimic an enhanced mass loading of a TO, causing  $f$  to decrease. However, any enhancement to the overall rigidity of the system should lead to a higher resonant frequency.<sup>16</sup> This point is illustrated with a simple model in Appendix A of this paper. Furthermore, we have carried out a finite-element method (FEM) calculation (see Appendix B) employing realistic parameters of the TO and solid helium in order to confirm this result. The positive correlation between  $c_{44}$  and  $f$ , their resemblances in the temperature dependence,<sup>23</sup> and the hysteresis common to both<sup>7,23</sup> all suggest that either the frequency

TABLE I. Approximate stress amplitudes corresponding to  $v_c$  in various cells. Values are estimated by ignoring the effects from the top and bottom surfaces of the cell and equating two different expressions for the torque:  $I\alpha = rA\sigma_0$ . Here,  $\alpha$  is the angular acceleration and  $A$  is the area at the rim of the cell. The stress exerted in an annular geometry differs from that in a cylindrical one by the approximate factor  $(2tf)_{\text{ann}}/(rf)_{\text{cyl}}$ .

Cell	$f$ [Hz]	$v_c$ [ $\mu\text{m s}^{-1}$ ]	$\sigma_c$ [mPa]
Cylinder <sup>a</sup>	1072	<3.5	<5.4
Cylinder <sup>b</sup>	1173	15	12
Cylinder <sup>b</sup>	496	15	28
Annulus <sup>c</sup>	912	3–40	1.6–22
Annulus <sup>d</sup>	912	10	5.4
Annulus <sup>e</sup>	874	40	3.3

<sup>a</sup>Present set of measurements.

<sup>b</sup>Data from Ref. 7.

<sup>c</sup>Data from Ref. 2.

<sup>d</sup>Data from Ref. 4.

<sup>e</sup>Data from Ref. 6.

shift is a direct consequence of the enhanced modulus and can be explained without invoking supersolidity or that the microscopic mechanism responsible for the NCRIF also affects the elastic properties of the solid (e.g., a recent suggestion is given in Ref. 24). The results presented below favor the latter.

In Sec. II we present our experimental observations in a general manner by simply describing the dependences of the observed frequency shifts and dissipation signals on temperature (see Figs. 1 and 2), oscillation speed<sup>25</sup> (see Fig. 3), and growth method. Two different interpretations of the data are given in Secs. III and IV. In the former we attempt to describe the experiments in the context of a supersolid that is permeated by vortices. Since vortex lines interact with velocity fields, one of the important parameters in this model is  $v_0$ . In Sec. V we discuss the consequences of attributing the entire frequency shift to an increase in the shear modulus of solid <sup>4</sup>He. It is assumed in this picture that the rigidity of the solid is strongly affected by the motion of dislocation lines under the applied stress  $\sigma_0$ . In anticipation of these two interpretations, we have simultaneously plotted the data in Fig. 3 as a function of  $v_0$  and  $\sigma_0$ . In addition, in both Figs. 4 and 5 we have plotted the frequency shift in terms of the NCRIF and  $\delta c_{44}/c_{44}$ .

## II. EXPERIMENTAL RESULTS

A recent study<sup>10</sup> of samples grown at constant temperature and pressure (CT and CP) at a single point on the solid-liquid coexistence curve found the onset of the frequency shift to be sharp and reproducible, which is consistent with the expected formation of single crystals. In contrast, wide variations in  $\delta f$  and  $T_o$  were observed when employing the blocked capillary (BC) method, which typically yields polycrystalline samples or highly strained crystals due to the pressure drop during freezing. In this paper we examine in

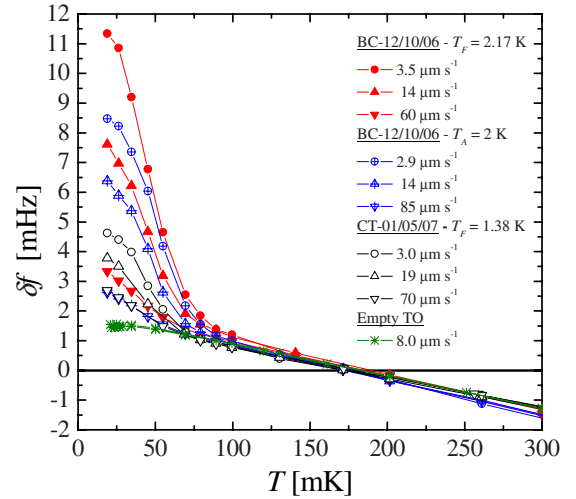


FIG. 1. (Color online) Temperature dependence of  $\delta f$  for a BC sample before and after annealing, and one CT sample. For all samples  $x_3 \approx 1$  ppb. Data were obtained with the beryllium-copper TO from Ref. 10. Freezing ( $T_F$ ) and annealing ( $T_A$ ) temperatures are given for each sample. All data were taken during cooling scans in which the temperature was successively lowered in controlled steps. For any one sample the measured frequency at  $T > T_o$  is identical for all values of  $v_0$ . For easy comparison we have set  $\delta f = 0$  at  $T = 175$  mK by subtracting 1071.007 Hz, 1071.011 Hz, 1071.035 Hz, and 1071.898 Hz from the data of BC-12/10/06, BC-12/10/06 post-annealing, CT-01/05/07, and the empty TO. Thus, the effective mass loading for each of these samples is 891 mHz, 887 mHz, and 863 mHz.

detail the different thermal histories of  $\delta f$  in BC and CT-CP samples that follow from changes in oscillation speed above and below  $T_o$ . We have measured the temperature dependence of  $\delta f$  in 30 samples, with the bulk of our work being carried out on “isotopically pure” ( $x_3 \approx 1$  ppb of <sup>3</sup>He) samples at  $1 \mu\text{m s}^{-1} < v_0 < 100 \mu\text{m s}^{-1}$ . To overlap with Ref. 7 we also studied two commercially pure ( $x_3 \approx 0.3$  ppm) samples up to speeds of  $880 \mu\text{m s}^{-1}$ .

Figure 1 shows the temperature dependence of  $\delta f$  for a BC sample before and after annealing, compared with that for a sample grown at CT. We find that the temperature de-

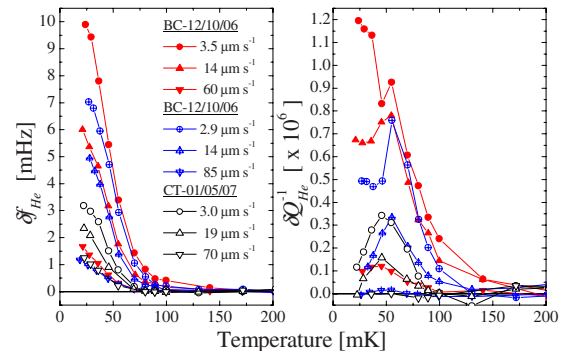


FIG. 2. (Color online) Temperature dependence of  $\delta f_{\text{He}}$  and  $\delta Q_{\text{He}}^{-1}$  for the same samples presented in Fig. 1, obtained by subtracting the temperature dependence of the empty cell. The symbols for BC-12/10/06, pre- and post-annealing, are identical to those in Fig. 1.

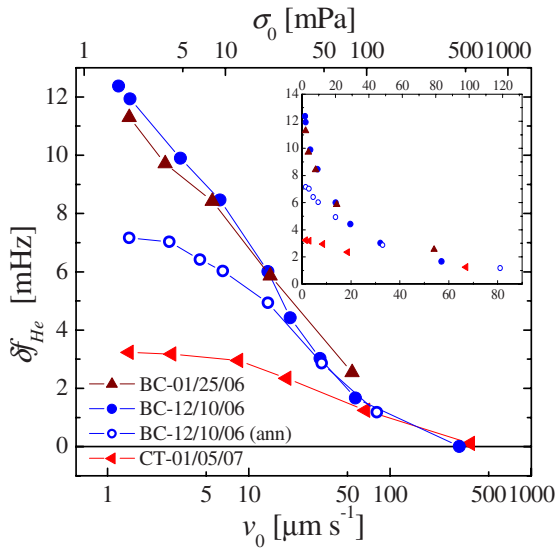


FIG. 3. (Color online) Dependence of the low-temperature value of  $\delta f_{\text{He}}$  on oscillation speed and applied stress. The inertial stress is approximated by  $\sigma_0 \approx \pi \rho f v_0 / 2$  for a given helium density  $\rho$ . Values of  $\delta f_{\text{He}}$  were extracted from cooling scans that began well above  $T_o$ . Samples are labeled according to growth method and date. The data are plotted versus a linear abscissa in the inset.

pendence of  $\delta f$  for each sample is reproducible in warming and cooling scans at low oscillation speeds—i.e., on the order of  $1 \mu\text{m s}^{-1}$ . Although the differences between BC and CT-CP samples are apparent at low speeds, the temperature dependence obtained at  $v_0 > 50 \mu\text{m s}^{-1}$  is very similar in all samples studied (including 0.3 ppm samples).

After subtracting the temperature dependence of the empty cell, we obtain the frequency shift and dissipation due

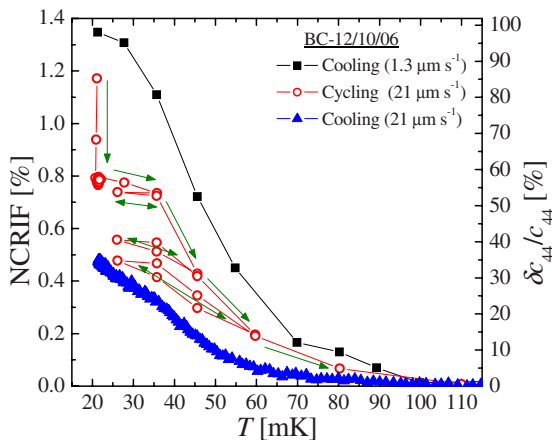


FIG. 4. (Color online) Metastability of  $\delta f_{\text{He}}$  (plotted as NCRIF and  $\delta c_{44}/c_{44}$ ) for a BC sample. The values of  $\delta c_{44}/c_{44}$  were calculated based on the assumption that the solid sample was isotropic—i.e., highly polycrystalline (Ref. 26) due to the BC method that was employed. Even larger values would be obtained if the sample was assumed to be a single crystal. Decay of the signal occurs for  $T > 30 \text{ mK}$ . Cycling above and below  $T^* = 30 \text{ mK}$  results in successively smaller values until equilibrium (i.e., that obtained when cooling from above  $T_o$ ) is reached. The speeds of  $v_0 = 1.3 \mu\text{m s}^{-1}$  and  $21 \mu\text{m s}^{-1}$  correspond to  $\sigma_0 = 2.0 \text{ mPa}$  and  $32 \text{ mPa}$ .

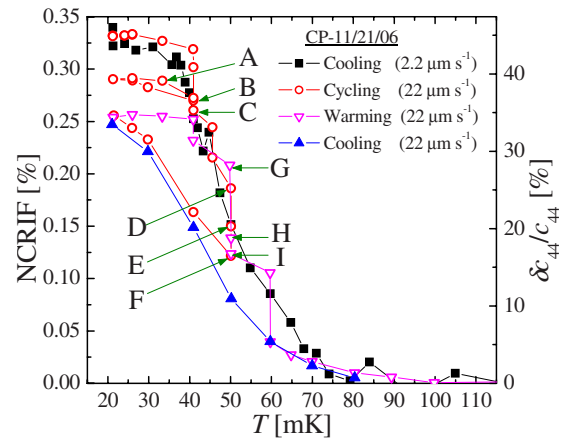


FIG. 5. (Color online) Metastability of the NCRIF and  $\delta c_{44}/c_{44}$  for a CP sample. The sample was assumed to be a single crystal with its  $c$  axis oriented horizontally. If we instead assume that the  $c$  axis is oriented vertically (or that the sample is isotropic), the low-temperature limiting value of  $\delta c_{44}/c_{44}$  would be 60% (30%). Labels A–I denote changes in the decay rate at several different temperatures. The speeds of  $v_0 = 2.2 \mu\text{m s}^{-1}$  and  $22 \mu\text{m s}^{-1}$  correspond to  $\sigma_0 = 3.4 \text{ mPa}$  and  $34 \text{ mPa}$ .

to solid  $^4\text{He}$ , which we respectively denote by  $\delta f_{\text{He}}$  and  $\delta Q_{\text{He}}^{-1}$ . These results are plotted in Fig. 2. There is considerable dissipation in rapidly grown BC samples even at the lowest temperatures. After annealing sample BC-12/10/06, the high-temperature tail of  $\delta f_{\text{He}}$  (and thus  $T_o$ ), the low-temperature limiting value of  $\delta f_{\text{He}}$ , and the magnitude of  $\delta Q_{\text{He}}^{-1}$  are all reduced. Thus it appears that annealing affects the temperature dependence of  $\delta f_{\text{He}}$  much in the same way as driving the TO at high speed (see Fig. 2). One difference, however, is that the results from annealing are permanent.

In Fig. 3 we have plotted the low-temperature value of  $\delta f_{\text{He}}$  measured at different  $v_0$ , which again demonstrates that the data converge at high speeds. One interesting difference from previous TO studies<sup>2,4,6–8</sup> is the lack of saturation in  $\delta f_{\text{He}}$  even well below  $10 \mu\text{m s}^{-1}$ . This is most evident in two BC samples (01/25/07 and 12/10/06) grown from the normal fluid phase, where  $\delta f_{\text{He}}$  actually doubles when  $v_0$  is decreased from  $10 \mu\text{m s}^{-1}$  to  $1 \mu\text{m s}^{-1}$ . In samples assumed to be of higher quality we find  $v_c \approx 3 \mu\text{m s}^{-1}$  ( $3.5 \mu\text{m s}^{-1}$  corresponds to  $\kappa = h/m$ ).

The curves in Fig. 3 were compiled from cooling scans that began well above the onset temperature. Using this procedure we found that  $\delta f_{\text{He}}$  is diminished at higher  $v_0$  for all  $T < T_o$  in a completely reproducible manner, whereas measurements taken during warming are history dependent when obtained at speeds greater than a few microns per second. As we will show below, varying the oscillation speed below the onset temperature can result in irreversible changes in  $\delta f_{\text{He}}$ . Careful examination of how the oscillation speed affects  $\delta f_{\text{He}}$  reveals metastability at the lowest temperatures, as depicted in Figs. 4 and 5 (see Secs. III and IV).

Using the following protocol, the thermal history of  $\delta f_{\text{He}}$  was investigated in crystals grown under different conditions. First, the temperature dependence of  $\delta f_{\text{He}}$  was measured while cooling at low speed ( $v_0 < 3 \mu\text{m s}^{-1}$ ). At  $T \approx 20 \text{ mK}$ ,  $v_0$  was slowly increased. Final velocities were

usually  $\sim 20 \mu\text{m s}^{-1}$ , but in some cases much greater (e.g., several hundred microns per second). Multiple thermal cycles were then performed in succession, indicated by the arrows in Fig. 4. Complete equilibration was purposely avoided while cycling between 30 mK and 60 mK in order to observe multiple metastable states. The measurement culminated with a high-velocity cooling trace that began well above  $T_o$ .

Figures 4 and 5 show that for one oscillation speed a number of different values of  $\delta f_{\text{He}}$  ( $\propto$  NCRIF and  $\delta c_{44}/c_{44}$ ) can be “frozen in” below a characteristic temperature  $T^* \approx 30$  mK. This is true regardless of the sample growth procedure. However, there are significant differences in the time evolution (following temperature steps) and the velocity dependence of  $\delta f_{\text{He}}$  between samples formed by the BC method and crystals grown at CT and CP. Similar behavior is seen in 0.3 ppm samples, but with  $T^* \approx 45$  mK. For all samples, there is no observable decay from any of the metastable states of  $\delta f_{\text{He}}$  on a time scale of days as long as the temperature is maintained below  $T^*$ . Further discussion of the hysteresis is deferred to Secs. III and IV below.

### III. VORTEX LIQUID MODEL

As stated in Sec. I, the TO experiments to date are qualitatively consistent with many features of Anderson’s vortex liquid model. The present work, however, demonstrates that below 60 mK the system does not act like a free vortex liquid as originally proposed. In fact, below 30 mK it exhibits severe pinning. With this picture in mind we can explain the temperature dependence of the NCRIF ( $\propto \delta f_{\text{He}}$ ) in Fig. 2, the velocity dependence in Fig. 3, and the history dependence in Figs. 4 and 5.

First we consider the temperature dependence. As the system is cooled through the transition, some number of free vortices are produced, which is proportional to  $v_0$ . When  $T \ll T_o$  the mobility of the existing vortices diminishes and it is unfavorable to create additional vortex lines. The inability of vortices to screen supercurrents leads to a sizable NCRIF in the low-temperature limit. When the system is driven at high speeds, not only is the NCRIF smaller, but the high-temperature tail of the NCRIF is reduced. This suggests that vortex pinning is very weak at  $T \geq 60$  mK. It is also likely that vortices are more easily excited as  $T_o$  is approached.

The velocity dependence in Fig. 3 reflects the distribution in the strength of individual vortex pinning sites at low temperature. Annealing might effectively remove the weakest pinning centers so that the low-temperature limiting value of the NCRIF is only decreased at small  $v_0$ . At greater speeds these weak regions are irrelevant since there is a plethora of free vortices, hence the convergence in Figs. 2 and 3 at  $v_0 > 50 \mu\text{m s}^{-1}$ .

In the context of superconductivity or magnetism (or superfluidity), the system is prepared differently if (velocity) field cooling or zero-field cooling is employed. The hysteresis shown in Figs. 4 and 5 is a consequence of what the authors of Ref. 7 have called vortex glass behavior. If the state of the system is prepared at low  $v_0$ , there are only a “small” number of vortices frozen into the solid. When  $v_0$  is

gradually increased while  $T < T^*$ , the NCRIF becomes either unstable (see Fig. 4) or metastable (see Fig. 5). In the former case, the NCRIF decays until it reaches a metastable state. For  $T > T^*$ , the NCRIF is reduced by the enhanced mobility of vortices.

The low-temperature metastability seems to depend on the difference between the initial NCRIF prepared at low speed and the “equilibrium” value obtained upon cooling at the higher speed. For instance, the difference is NCRIF = 0.9% for BC-12/10/06 (see Fig. 4) and NCRIF = 0.08% for CP-11/21/06 (see Fig. 5), resulting in a much more stable value for the latter. The measured value for BC-12/10/06 immediately drops by about 40% of its magnitude following the increase in  $v_0$ , while there is no change for CP-11/21/06. The behavior of CP-11/21/06 is similar to that in Ref. 7, which was compared with the Meissner effect (i.e., a robust NCRIF due to the inability of vortices to enter into the solid). We note that the metastability up to  $800 \mu\text{m s}^{-1}$  in Ref. 7 may be related to the small NCRIF ( $\approx 0.1\%$ ) of the sample. In comparison, upon raising  $v_0$  up to  $880 \mu\text{m s}^{-1}$  we observe, for an  $x_3 = 0.3$  ppm sample with NCRIF  $> 1\%$  ( $\delta f_{\text{He}} > 8$  mHz), an abrupt drop in the signal that is followed by a gradual decay. In fact, in this extreme limit of  $v_0$ , the decay rate is essentially insensitive to temperature steps (warming and cooling) between 20 mK and 45 mK. Only upon warming above 60 mK does the decay rate increase further.

In 1 ppb samples, the stability is reduced as the temperature is raised above 30 mK. Fragments of data from scans of CP-11/21/06 are displayed in Fig. 6. The data at any  $T < 60$  mK cannot be fit satisfactorily using a simple mathematical formula. For example, the decay at 40 mK in Fig. 6(a) (between points A and B) begins immediately, but slows down abruptly after only 1 h. In Fig. 6(b), the NCRIF barely changes in the first hour at the same temperature (data prior to point G). Irregular rates are even more apparent at 50 mK. The decay slows down dramatically when NCRIF crosses (e.g., points E and H) from the region above the low-velocity cooling trace to the region below it. This is most obvious in Fig. 6(b), where the sample was warmed to 50 mK rapidly to result in a larger initial NCRIF. The very different decay rates in these two regions and the identical temperature dependence in warming and cooling scans both suggest that there is physical significance to the reproducible data obtained in the low-velocity limit. Similar behavior could not be observed in BC samples because of higher decay rates; i.e., it was impossible to exceed the low-velocity trace upon warming (see Fig. 4).

Interestingly, the decay in CP-11/21/06 at 60 mK (data following point I) is different from that at 40 mK and 50 mK in that it can be well fit to an exponential form, which yields a time constant of 2.25 h. The smooth decay across the low-velocity trace may indicate that the small tail of the NCRIF for  $T \geq 60$  mK does not denote the same “boundary” as seen at lower temperatures. This observation is complemented by the enhanced decay rate at 60 mK that we find in 0.3 ppm samples, as well as the  $x_3$ -independent specific heat peak that has been observed<sup>19</sup> in the same vicinity, and suggests that there is some inherent transition between the “free” and “pinned” regimes.

Another intriguing result is the nearly equal spacing between each metastable NCRIF among the four samples that

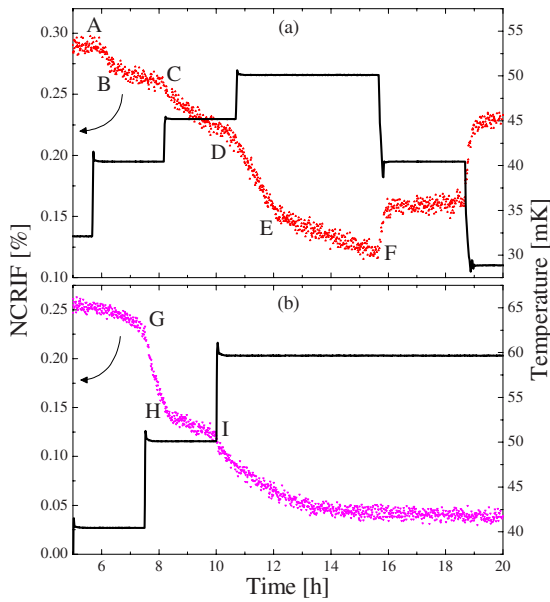


FIG. 6. (Color online) Segments of raw data used to compile the “cycling” and “warming” curves in Fig. 5. Decay rates above ( $D-E$  and  $G-H$ ) the low-velocity trace are greater than those below ( $E-F$  and  $H-I$ ). The ordinate axis is given in terms of the NCRIF for easy comparison with Fig. 5.

we studied in detail (e.g., see Figs. 4 and 5). It is clear that the system prefers to possess specific values of the NCRIF in the low-temperature limit. For example, counter to the slow decay upon warming a solid sample, as the temperature is lowered, we find the NCRIF to “jump” up to a steady value (see the data in Fig. 6 following point  $F$ ). If we naively estimate the frequency shift due to the presence of a single vortex line using the expression<sup>27</sup>  $I_{\text{vort}} = \pi\rho r^4(\text{NCRIF})/\ln[r/a_0]$ , we calculate a shift corresponding to 25% of the observed NCRIF for a vortex core radius<sup>28</sup> of  $a_0=0.1$  nm. This value is of the same order of magnitude to what we observe (e.g., from Fig. 5 we get  $0.04/0.33=11\%$  for CP-11/21/07).

Although our experimental results can be qualitatively interpreted within the framework of Anderson’s vortex liquid model, very few quantitative comparisons are possible.<sup>29</sup> One of the present experimental results that is difficult to understand in the vortex picture is depicted in Fig. 3. In two samples the observed frequency shift continues to increase when  $v_0$  is reduced to  $1 \mu\text{m s}^{-1}$ , such that even the peak-to-peak amplitude of  $2 \mu\text{m s}^{-1}$  is less than that which corresponds to a single quantum of circulation ( $\sim 3.5 \mu\text{m s}^{-1}$ ).

#### IV. ANOMALOUS ELASTICITY OF SOLID $^4\text{He}$

Due to the similarities discussed in Sec. I between the observed frequency shifts and the results of Ref. 23, we are compelled to try to interpret the data from Sec. II in terms of the response of the dislocation network to oscillating stress fields imposed on the solid.

Here we report our preliminary estimates of changes in the shear modulus of solid  $^4\text{He}$ . By determining the  $c_{44}$

dependence of the TO resonant frequency, we are able to extract estimates of changes in the modulus that are necessary to account for the experimental  $\delta f_{\text{He}}$  values (see Appendix B). The change is given by  $\delta c_{44}/c_{44} = (d \ln f / d \ln c_{44})^{-1} (\delta f_{\text{He}} / f)$ , where the derivative term comes from the FEM calculation. The results of our calculations are shown in Figs. 4 and 5. Since the low-temperature change in the resonant frequency is very small (parts per million), it scales linearly with the change in the shear modulus. As a result, the inferred temperature dependence of  $\delta c_{44}/c_{44}$  is identical to  $\delta f_{\text{He}}$ . It is therefore natural that the qualitative features of the data in Ref. 23 be very similar to that from TO studies, as was mentioned in Sec. I.

In addition to temperature, Day and Beamish found the measured shear modulus to be a function of stress amplitude. Below a critical stress  $\sigma_c$  the magnitude of  $c_{44}$  saturates at a maximum value, as does  $\delta f_{\text{He}}$  in some samples (see Fig. 3). This critical value  $\sigma_c=300$  mPa is smaller than the estimated breakaway stress of 4 Pa for a  $^3\text{He}$ - $^3\text{He}$  separation of  $5 \mu\text{m}$  (a typical loop length<sup>18,21,30</sup>) along a dislocation, but closely matches the stress at which  $\delta f_{\text{He}}$  tends to zero in Fig. 3. Such strong nonlinearity between the drive and response, also seen in other low-frequency acoustic measurements,<sup>31</sup> occurs at “critical” speeds that are 100–1000 times less (e.g.,  $\sim 50 \text{ nm s}^{-1}$  in Ref. 23) than in TO studies.<sup>2,4,6–8</sup> (see Table I). It was concluded in Ref. 23 that  $\sigma_c$  is a more fundamental quantity than  $v_c$  due to it being independent of the measurement frequency. However, this appears inconsistent with Ref. 7 and implies that the two types of measurements, although clearly related on some level, are distinct.

Another quantitative difference between Ref. 23 and TO studies is the magnitude of the relative change in  $c_{44}$ . In order to account for the observed  $\delta f_{\text{He}}$  in TO measurements, the required  $\delta c_{44}/c_{44}$  values among the samples studied here are between 2 and 5 times larger than the greatest of that seen in Ref. 23. Moreover, the changes are greater than the theoretical upper limit of 30% that can result from the pinning of dislocation lines.<sup>32</sup> We have carried out similar calculations for some of the TOs in the literature<sup>2,7,33</sup> and found that even larger values of  $\delta c_{44}/c_{44}$  are necessary to account for the observed  $\delta f_{\text{He}}$ . For instance, typical NCRIF values in Refs. 2 and 33 translate into approximate increases in  $c_{44}$  by factors of 20 and 3, respectively. We obtain a factor of 4 for the antisymmetric (high- $f$ ) mode of the double oscillator from Ref. 7. For the symmetric (low- $f$ ) mode, the experimental frequency shift corresponds to a factor of 2 increase in  $c_{44}$ . This implies that the size of the effect depends on frequency, contrary to the findings of Day and Beamish.

A control experiment was carried out in the original study by Kim and Chan.<sup>2</sup> In particular, measurements were taken in a cell where a physical barrier was inserted into the annular helium space. The idea behind this control is that if the frequency shift in the barrier-free cell is due to superflow, then in the “blocked cell”  $\delta f_{\text{He}}$  should be greatly reduced since the flow path is extremely tortuous. If, on the other hand, the observed shift is due to some “local” effect, unrelated to macroscopic phase coherence across the entire helium sample,  $\delta f_{\text{He}}$  should not be very different in the two cells. The apparent NCRIF in the blocked cell was found to be about 65 times smaller than the expected NCRIF of

$\sim 1.4\%$  (the average value obtained with the barrier-free cell in the same study), which is consistent with calculations of tortuous superflow.<sup>34</sup> A drawback of this control experiment is that the physical dimensions of the barrier-free annulus (10 mm o.d.  $\times$  0.95 mm width  $\times$  6.35 mm height) and the blocked annulus (15 mm o.d.  $\times$  1.1 mm width  $\times$  5.0 mm height) are not identical. Moreover, it has been shown that, despite identical growth conditions, very different NCRIF values are attainable in different TOs.<sup>10</sup>

Since it is unclear what the consequences would be for the enhanced shear modulus in either configuration, FEM simulations were carried out for four different situations: on the two real TOs (barrier-free and blocked cells) from Ref. 2 and on two “hypothetical” TOs with dimensions identical to the real ones except with a barrier inserted into the helium space of the barrier-free cell and removed from the blocked cell. We found the frequency shift caused by an increase in  $c_{44}$  for both TOs to be essentially indifferent to the presence or absence of the barrier. This is important since it means that the blocked-cell control experiment can distinguish between NCRI and changes in the shear modulus. For the barrier-free cell we calculated that  $\delta f_{\text{He}}/f \approx 0.4$  ppm for a 20% increase in  $c_{44}$ , both with and without the barrier. For the same  $\delta c_{44}/c_{44}$  and irrespective of the barrier, we found for the blocked cell that  $\delta f_{\text{He}}/f \approx 0.1$  ppm. In order to explain the observed frequency shifts from Ref. 2 as unrelated to the onset of NCRI, increases in  $c_{44}$  by a factor of 20 and 2 for the barrier-free and blocked cells, respectively, are necessary.

It is worth mentioning that this control experiment has recently been repeated<sup>33,35</sup> using a clever modification to Kim and Chan’s original experimental design, so as to allow for the barrier-free and blocked configurations to be examined within the same cell. Rittner and Reppy found that the insertion of two barriers eliminated the frequency shift, which in the open geometry corresponded to NCRIF=16%. These two blocked annulus experiments,<sup>2,35</sup> in conjunction with our FEM studies, offer the strongest support for interpreting the frequency shift observed in various TO studies as a consequence of superflow.

We note that it is also difficult to apply the dislocation pinning picture to the experiments in porous Vycor glass,<sup>1</sup> in which the dimensions of helium (i.e., the pore size) are smaller than typical dislocation loop lengths in bulk crystals.<sup>18,21,30</sup> This, and the fact that the crystalline phase<sup>36</sup> of the confined  $^4\text{He}$  is body-centered-cubic rather than hexagonal-close-packed, would lead one to expect very different behavior in the response to torsional oscillations, contrary to what is observed.

In addition to dislocations, it is possible that  $^3\text{He}$  impurities can hinder the motion of other topological defects within the sample, such as grain boundaries. A theoretical approach to the problem is likely much more complicated (and less general) than that used to describe dislocation motion. The simplest attempt might be to treat a grain boundary as an array of dislocation lines, which should therefore be less mobile than a single line. We are unaware of any studies clearly demonstrating the mobility of grain boundaries away from the solid-liquid coexistence curve. Due to the lack of theory and experiment specific to helium crystals, it is very difficult

to gauge what range of impurity concentrations, temperatures, and frequencies are relevant to the problem.

## V. CONCLUSIONS

We have studied a number of solid  $^4\text{He}$  samples grown within a torsional oscillator at constant temperature and pressure, as well as with the blocked-capillary method, and found that the resonant frequency of the system possesses a very strong thermal history. The magnitude of the apparent NCRIF measured in the low-temperature limit is reproducible when obtained upon cooling the sample from temperatures well above the transition. Modulation of the oscillation speed below the onset temperature reveals the existence of many metastable states.

We find that these properties are qualitatively consistent with two different interpretations: the response of vortices to velocity fields and/or the response of dislocation lines within the solid to oscillating stress fields. The mobility of either or both of these entities becomes very limited with decreasing temperature, resulting in hysteretic behavior below 60 mK. Extreme pinning takes place below 30 mK ( $x_3=1$  ppb) or 45 mK ( $x_3=0.3$  ppm), such that their motion is essentially frozen out.

The increase of the TO resonant frequency at low temperature found in this and other TO studies is consistent with superflow of solid  $^4\text{He}$ . A number of the experimental details can be understood in terms of the vortex liquid picture proposed by Anderson. One notable puzzle appears to be the very low critical velocity found in this study. There are clear limitations to interpreting the observed frequency shifts solely in terms of the stiffening of the dislocation network in solid  $^4\text{He}$ . More experimental and theoretical efforts are needed to understand the exact connection between NCRI and enhanced shear modulus.

## ACKNOWLEDGMENTS

We thank P. W. Anderson, J. R. Beamish, W. F. Brinkman, Z. Cheng, D. A. Huse, J. Jain, H. Kojima, X. Lin, N. Mulders, L. Pollet, N. V. Prokof’ev, A. S. C. Rittner, J. Toner, and J. T. West for their input. We are grateful to J. A. Lipa for providing us with isotopically pure  $^4\text{He}$ . Funding was provided by the NSF under Grant No. DMR-0207071 and No. DMR-0706339.

## APPENDIX A: A SIMPLE ANALYTICAL MODEL

Consider a TO with internal cylindrical space of radius  $r$  and height  $l$  available for  $^4\text{He}$ . We can estimate the functional dependence and overall sensitivity of  $f$  to  $c_{44}$ . For simplicity we ignore the effects from the top and bottom of the cell and only consider the shear response of  $^4\text{He}$  to rotation of the outer wall. For the given geometry one finds that the solution to the wave equation is proportional to

the Bessel function  $J_1(kr)$ , where  $k=2\pi f/v_t$ . From this we can calculate the angular component of the traction,

$$\frac{dF_\theta}{dA} = c_{44}C \left( kJ_1'(kr) - \frac{J_1(kr)}{r} \right), \quad (\text{A1})$$

where  $C$  is a coefficient to the Bessel function that is defined by the boundary conditions (in the derivation below,  $C$  conveniently drops out of the problem). At the outer boundary the torque is given by

$$N_{\text{He}} = (r)(2\pi r l) \left( \frac{dF_\theta}{dA} \right). \quad (\text{A2})$$

The impedance is defined by the ratio of the torque and the angular velocity,

$$Z_{\text{He}} = \frac{rN_{\text{He}}}{i2\pi f C J_1(kr)} = i \frac{8\pi f I_{\text{He}}}{k^2 r^2} \left( 1 - \frac{krJ_1'(kr)}{J_1(kr)} \right), \quad (\text{A3})$$

where  $I_{\text{He}} = \rho\pi r^4 l/2$ . Upon expanding the Bessel functions we find that

$$Z_{\text{He}} \approx i2\pi f I_{\text{He}} \left( 1 + \frac{k^2 r^2}{24} \right). \quad (\text{A4})$$

The ‘‘additional’’ mass loading  $k^2 r^2 I_{\text{He}}/24$  is zero in the limit of infinite sound speed. However, for  $v_t \approx 260 \text{ m s}^{-1}$  this term is roughly  $6 \times 10^{-4}$  for our TO. In the extreme (non-physical) case of  $v_t$  transitioning to infinity, the measured mass loading would change by this fraction and thus mimic the scenario where  $\text{NCRIF}=0.06\%$ .

In order to estimate  $\delta f_{\text{He}}$  for any change in  $v_t$  or  $c_{44}$ , we can go one step further and solve for the resonance condition  $Z=0$ , where  $Z$  is the total impedance of the oscillator that possesses terms that include the torsion spring constant  $K$  and empty cell moment of inertia  $I$ . The net result is

$$\frac{\delta f_{\text{He}}}{f} \approx \left( \frac{I_{\text{He}}}{I + I_{\text{He}}} \frac{\pi^2 \rho r^2 f^2}{12 c_{44}} \right) \frac{\delta c_{44}}{c_{44}} \approx (5 \times 10^{-7}) \frac{\delta c_{44}}{c_{44}}. \quad (\text{A5})$$

## APPENDIX B: DERIVATION OF ELASTIC PROPERTIES FROM THE FINITE-ELEMENT METHOD

An eigenfrequency analysis of our TO was carried out using the Structural Mechanics Module of COMSOL Multiphysics. The entire TO (the base, torsion rod, and torsion bob both with and without  $^4\text{He}$ ) was drawn in a computer-aided design (CAD) environment, from which a mesh of finite, tetrahedral elements was generated. To perform calculations in a convenient period of time, the number of elements was typically limited to less than 30 000. However, meshes with higher densities were also tested in several cases to ensure the accuracy of the resonant frequency. Based only on the dimensions of the TO and the elastic properties of its constituents, we found  $f$  to be in excellent agreement with the experimental value (i.e., within 1%). Similarly, high accuracy was obtained for the calculated mass loadings of a number of samples (within 2%).

Further details of our presently ongoing FEM study will be published elsewhere. In essence, we obtain the resonant frequency of the TO using different values of  $c_{44}$  for solid  $^4\text{He}$ , thus giving  $f(c_{44})$ . We find the frequency calculated with the FEM to scale linearly with  $c_{44}$ , as one should expect for small changes. A simple Taylor expansion yields

$$f(c_{44} + \delta c_{44}) = f(c_{44}) + \delta f_{\text{He}} \approx f(c_{44}) + \delta c_{44} \frac{df}{dc_{44}}. \quad (\text{B1})$$

Therefore,

$$\frac{\delta f_{\text{He}}}{f} \approx \frac{\delta c_{44}}{c_{44}} \frac{df}{dc_{44}} = \frac{d \ln f}{d \ln c_{44}} \frac{\delta c_{44}}{c_{44}}. \quad (\text{B2})$$

The magnitude of  $d \ln f / d \ln c_{44}$ , which is obtained from the FEM calculations, varies between  $\sim 5$  and  $\sim 10$  parts in  $10^6$  [about 10 times larger than the estimate in Eq. (A5)].

We are able to infer changes in the shear modulus of solid  $^4\text{He}$  by combining the derivative term with experimentally measured frequency shifts. The vertical axes on the right-hand side of both Figs. 4 and 5 are derived by inverting Eq. (B2),

$$\frac{\delta c_{44}}{c_{44}} \approx \left( \frac{d \ln f}{d \ln c_{44}} \right)^{-1} \frac{\delta f_{\text{He}}}{f}. \quad (\text{B3})$$

Finally, we note that one can also gain some information on changes to the sound attenuation  $\alpha$  in  $^4\text{He}$ . If we include the first imaginary term in the Taylor expansion, we get

$$f(\tilde{c}_{44}) = f(c_{44} + \delta c_{44} + i\beta) \approx f(c_{44} + \delta c_{44}) + i\beta \frac{df}{dc_{44}}, \quad (\text{B4})$$

where  $\beta$  is the complex component of the linear response modulus. For a relaxation process of characteristic time scale  $\tau$  we can relate  $\beta$  to  $\alpha$  using the definition of transverse sound  $v_t$ ,

$$\frac{c_{44} + i\beta}{\rho} = v_t^2 (1 + i2\pi f \tau) \approx v_t^2 \left( 1 + i \frac{\alpha v_t}{\pi f} \right), \quad (\text{B5})$$

where  $\rho$  is the density of  $^4\text{He}$  and we have assumed that  $2\pi f \tau \ll 1$ . The imaginary term in the complex shear modulus affects the  $Q$  through the expression

$$f \left( 1 + \frac{i}{2Q} \right) \approx f(c_{44} + \delta c_{44}) + i\beta \frac{df}{dc_{44}}. \quad (\text{B6})$$

Since dissipation is additive, we gain access to the temperature dependence of  $\alpha$  in helium if we subtract the empty cell data. Thus, from the above equations it is only a matter of algebra to show that

$$\delta \alpha \approx \frac{\pi f}{2v_T} \left( \frac{d \ln f}{d \ln c_{44}} \right)^{-1} \delta Q_{\text{He}}^{-1}. \quad (\text{B7})$$

As an example, Eq. (B7) results in a maximum value of  $\delta \alpha \approx 5 \times 10^{-3} \text{ cm}^{-1}$  (at  $v_0 \approx 3 \text{ } \mu\text{m s}^{-1}$ ) for all three samples shown in Fig. 2.

- \*Present address: Department of Physics, University of Basel, CH-4056 Basel, Switzerland; cctonyl@gmail.com
- <sup>1</sup>E. Kim and M. H. W. Chan, *Nature (London)* **427**, 225 (2004).
  - <sup>2</sup>E. Kim and M. H. W. Chan, *Science* **305**, 1941 (2004).
  - <sup>3</sup>E. Kim and M. H. W. Chan, *J. Low Temp. Phys.* **138**, 859 (2005).
  - <sup>4</sup>E. Kim and M. H. W. Chan, *Phys. Rev. Lett.* **97**, 115302 (2006).
  - <sup>5</sup>Ann Sophie C. Rittner and J. D. Reppy, *Phys. Rev. Lett.* **97**, 165301 (2006).
  - <sup>6</sup>Ann Sophie C. Rittner and J. D. Reppy, *Phys. Rev. Lett.* **98**, 175302 (2007).
  - <sup>7</sup>Y. Aoki, J. C. Graves, and H. Kojima, *Phys. Rev. Lett.* **99**, 015301 (2007).
  - <sup>8</sup>A. Penzev, Y. Yasuta, and M. Kubota, *J. Low Temp. Phys.* **148**, 677 (2007).
  - <sup>9</sup>M. Kondo, S. Takada, Y. Shibayama, and K. Shirahama, *J. Low Temp. Phys.* **148**, 695 (2007).
  - <sup>10</sup>A. C. Clark, J. T. West, and M. H. W. Chan, *Phys. Rev. Lett.* **99**, 135302 (2007).
  - <sup>11</sup>E. Kim, J. S. Xia, J. T. West, X. Lin, A. C. Clark, and M. H. W. Chan, *Phys. Rev. Lett.* **100**, 065301 (2008).
  - <sup>12</sup>A. Penzev, Y. Yasuta, and M. Kubota, arXiv:0711.0212 (unpublished).
  - <sup>13</sup>P. W. Anderson, *Nat. Phys.* **3**, 160 (2007).
  - <sup>14</sup>We note an error in Refs. 2 and 4—i.e.,  $t=0.95$  mm, rather than 0.6 mm.
  - <sup>15</sup>It is known that  $^3\text{He}$  atoms are attracted to vortices in superfluid liquid  $^4\text{He}$  due to the lower local density in the vortex core. For this reason it has been suggested that vortices in solid  $^4\text{He}$  are nucleated between lattice sites in regions of lower density. For instance, see W. M. Saslow, *Phys. Rev. B* **71**, 092502 (2005). Repulsion of  $^3\text{He}$  atoms from the vortex core is expected if the local density is higher than the average value. This might in fact be applicable to solid  $^4\text{He}$  if the supersolid phase is due to a finite concentration of vacancies. For example, see C. Wu, H. Chen, J. Hu, and S. C. Zhang, *Phys. Rev. A* **69**, 043609 (2004).
  - <sup>16</sup>Z. Nussinov, A. V. Balatsky, M. J. Graf, and S. A. Trugman, *Phys. Rev. B* **76**, 014530 (2007).
  - <sup>17</sup>A. V. Balatsky, M. J. Graf, Z. Nussinov, and S. A. Trugman, *Phys. Rev. B* **75**, 094201 (2007). We note that the particulars of the theory are not quite reconciled by the observed frequency dependence of  $\delta f$ . For example, based on the glass parameters obtained from the symmetric mode of oscillation in Ref. 7, the predicted frequency shift of the antisymmetric mode is approximately 10 times smaller than the experimental value.
  - <sup>18</sup>R. Wanner, I. Iwasa, and S. Wales, *Solid State Commun.* **18**, 853 (1976).
  - <sup>19</sup>X. Lin, A. C. Clark, and M. H. W. Chan, *Nature (London)* **449**, 1025 (2007).
  - <sup>20</sup>M. G. Richards, J. Pope, and A. Widom, *Phys. Rev. Lett.* **29**, 708 (1972); V. N. Grigoriev *et al.*, *J. Low Temp. Phys.* **13**, 65 (1973); A. R. Allen, M. G. Richards, and J. Schratte, *ibid.* **47**, 289 (1982).
  - <sup>21</sup>I. Iwasa and H. Suzuki, *J. Phys. Soc. Jpn.* **49**, 1722 (1980).
  - <sup>22</sup>M. A. Paalanen, D. J. Bishop, and H. W. Dail, *Phys. Rev. Lett.* **46**, 664 (1981).
  - <sup>23</sup>J. Day and J. R. Beamish, *Nature (London)* **450**, 853 (2007).
  - <sup>24</sup>J. P. Bouchund and G. Biroli, arXiv:0710.3087v2 (unpublished).
  - <sup>25</sup>We discuss the “velocity dependence” in a general sense, in that it is simply proportional to the drive level input to the system (as is amplitude, acceleration, stress, etc.).
  - <sup>26</sup>J. E. Vos *et al.*, *Physica* **37**, 51 (1967).
  - <sup>27</sup>G. B. Hess, *Phys. Rev.* **161**, 189 (1967).
  - <sup>28</sup>Due to the logarithmic dependence, the magnitude of the vortex angular momentum is fairly insensitive to  $a_0$  (e.g., taking  $a_0 = 100$  nm would reduce the calculated frequency shift by less than a factor of 2).
  - <sup>29</sup>A very recent attempt at an in-depth analysis has been made in Ref. 12. If we plot our data in the same manner as Fig. 3 in Ref. 12, we observe very different behavior. At present, we do not understand this discrepancy. However, it is interesting to note that for such plots we see qualitative differences between CT-CP and BC samples.
  - <sup>30</sup>I. Iwasa, K. Araki, and H. Suzuki, *J. Phys. Soc. Jpn.* **46**, 1119 (1979).
  - <sup>31</sup>Yu. Mukharsky, O. Avenel, and E. Varoquaux, *J. Low Temp. Phys.* **148**, 689 (2007).
  - <sup>32</sup>We note that Paalanen, Bishop, and Dail (Ref. 22) previously reported a 40% change in the shear modulus, but this included high-temperature data near the melting point where there are likely other stiffening processes to account for (e.g., the presence or absence of thermally activated vacancies).
  - <sup>33</sup>Calculations were also done for a TO now being used by Rittner and Reppy at Cornell University. The construction is similar to that used in Ref. 6, but with a slightly simpler design that is easier to model accurately.
  - <sup>34</sup>E. J. Mueller (private communication).
  - <sup>35</sup>A. S. C. Rittner, *Bull. Am. Phys. Soc.* **53**, 5 (2008).
  - <sup>36</sup>D. Wallacher, M. Rheinstaedter, T. Hansen, and K. Knorr, *J. Low Temp. Phys.* **138**, 1013 (2005).